

Following up Fermi GBM Gamma-Ray Bursts

V. Connaughton, and M. S. Briggs
University of Alabama, Huntsville

A. Goldstein (NASA Postdoctoral Fellow)
NASA Marshall Space Flight Center

Abstract

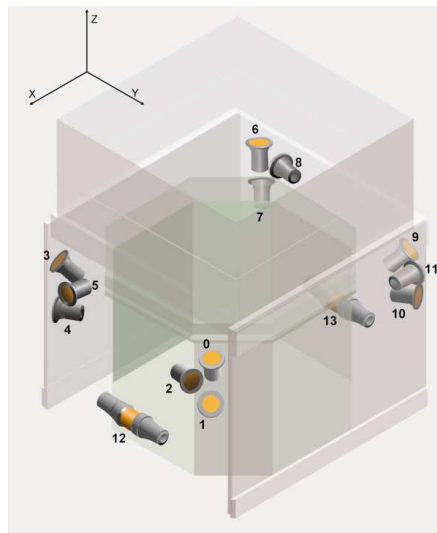
The *Fermi* Gamma-Ray Burst Monitor (GBM) has been detecting 240 Gamma-Ray Bursts (GRBs) per year since 2008, 40-45 of them per year short GRBs. GBM is an all-sky transient monitor of the hard X-ray sky operating between 8 keV and 40 MeV. GBM localizes sources by triangulating the most likely source position based on observed count rates in detectors with different orientations to the sky. GRB locations are disseminated using GRB Coordinate Network (GCN) notices. We report here an analysis of over 300 GBM localizations for which more accurate positions are known. Systematic uncertainties of about $2 - 4^\circ$ affect about 90% of GBM localizations (68% confidence level), with larger systematic effects for the remaining 10%. These systematic components are added in quadrature to the statistical uncertainties of $1 - \sim 10^\circ$ and provided as probability maps to the follow-up community an hour or less after the GRB trigger. The intermediate Palomar Transient Factory (iPTF) has used these maps to detect three GRB afterglows using the GBM positional information.

1 The *Fermi* Gamma-Ray Burst Monitor

GBM is a collection of 14 uncollimated scintillators on-board the *Fermi* spacecraft [1]. Because of Earth occultation and passages through the South Atlantic Anomaly, each position on the sky is viewed by GBM with approximately a 50% duty cycle. Energy coverage from 8 - 1000 keV is provided by 12 Sodium Iodide (NaI) detectors, with two Bismuth Germanate detectors covering the range from 200 keV to 40 MeV. GBM triggers on a GRB when count rates in two or more of the NaI detectors significantly exceed background levels on one or more timescales from 16 to 4096 ms, usually in the 50 - 300 keV energy range. Other triggering energy ranges provide sensitivity to a variety of transient phenomena: solar flares and soft gamma-ray repeaters at the low end and terrestrial gamma-ray flashes at higher energies. The arrangement of GBM detectors on the *Fermi* spacecraft is shown in Figure 1. Source localization

is done by minimizing χ^2 on a grid of 41168 points on the sky, comparing the observed background-subtracted count rates in each of the 12 NaI detectors with model rates obtained by convolving the detector response with three representative GRB spectra. The spectrum that returns the lowest χ^2 in the minimization is assumed to best represent the GRB spectrum and the sky position minimizing χ^2 for that model spectrum is selected as the most likely position for the GRB. Locations are produced on-board, by the flight software, and on the ground, from data downlinked within seconds of the GRB trigger (ground-auto) or with a larger data set and human intervention (human-in-the-loop, or HitL). Flight software and ground-auto locations are distributed as GCN notices from 10– \sim 45 s following the trigger, with ground-auto locations being significantly more accurate owing to the availability of finer sky grid resolutions and more varied spectral shapes for model comparison on the ground. The HitL locations have latencies from 20 min to over an hour following the trigger and are also distributed as GCN notices. The suite of localizations, from flight software to human-in-loop, allows the follow-up community to optimize their observation strategy, with wide-field instruments, capable of rapid response but shallow coverage, more suited to chasing the automated locations, and more sensitive instruments that are less capable of covering large sky areas waiting for the HitL locations.

Figure 1: Arrangement of GBM detectors on *Fermi*. The 12 NaI (numbered 0 - 11) and 2 BGO (12 - 13) detectors are mounted on the +X and -X axes in the *Fermi* coordinate system. The Large Area Telescope (LAT) boresight is along the Z axis.

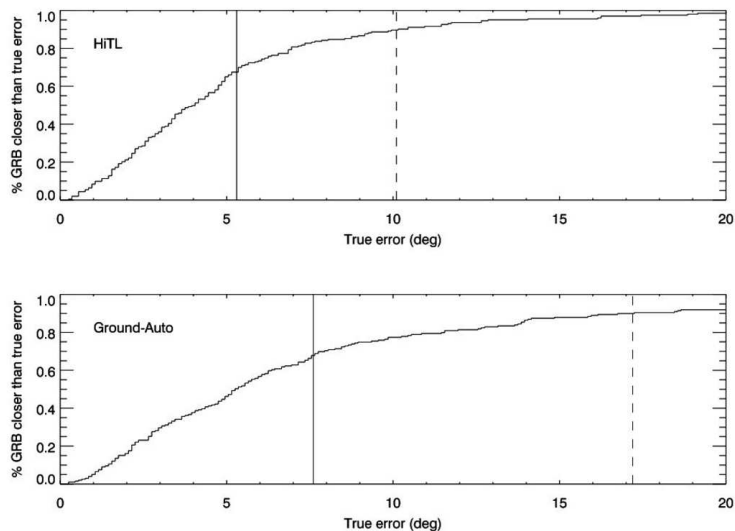


2 GBM location offsets from known positions

We use 203 GRBs localized by *Swift*, LAT, INTEGRAL, MAXI and SuperAGILE to analyze the accuracy of GBM GRB localizations. Figure 2 shows the fraction of GRBs as a function of the distance from the known position for the HitL and ground-

auto locations, regardless of the reported uncertainty on the localization. There can be several ground-auto locations, with updates for bursts showing brighter episodes following the initial localization. We use the last-reported ground-auto location, with the lowest statistical uncertainty. It can be seen that 68% of the ground-auto locations lie within 7.6° of the true position, with 90% within about 17° . The more refined HitL positions are significantly more accurate, with 68% within 5.2° of the true position and 90% within 10° , at the cost of a longer latency of at least 20 minutes. If we consider the reported statistical uncertainties, then for both the ground-auto and the HitL localizations, the 68% uncertainty regions contain the true position $\sim 40\%$ of the time and the 95% uncertainty regions 70% of the time. This implies there is a systematic component to the total uncertainty on the calculated burst position.

Figure 2: Accuracy of GBM localizations. The cumulative distributions show the fraction of GBM localizations as a function of offset in degrees from a known GRB location. The solid and dashed vertical lines show, respectively, the containment radius for 68% and 90% of the reference positions. The top panel is for the HitL locations, the bottom for the latest ground-auto location.

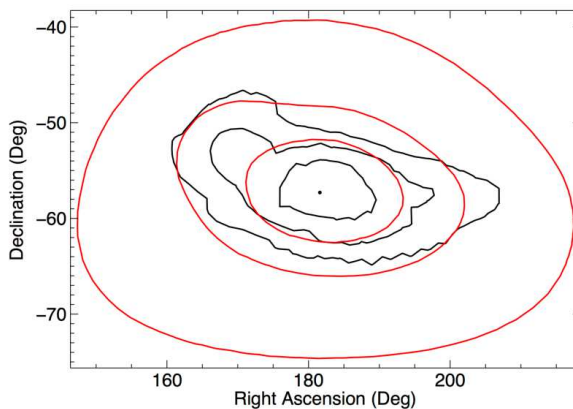


We augment the 203 reference positions with 9 intersecting annuli and 100 single annuli from InterPlanetary Network triangulations. A Bayesian approach used to characterize the systematic uncertainties in Burst And Transient Source Experiment (BATSE) GRB localizations [2] was then applied to the 312 GBM GRBs with reference locations. A preference for a model with two Gaussian components was found, with a core of about 90% of GRB localizations centered on $3.7^\circ \pm 0.2^\circ$ and a tail centered on $14.3^\circ \pm 2.5^\circ$. A core-plus-tail model was also favored for the BATSE GRB sample. We find a dependence for the systematic error in the core of the sample on the burst geometry in the spacecraft frame. Bursts from directions along the $\pm Y$ axes have smaller errors ($2.3^\circ \pm 0.4^\circ$) than those incident along the $\pm X$ axes ($4.1^\circ \pm 0.3^\circ$), with the fraction of GRBs in the core and the errors in the tail similar for both geometries [3].

3 Localization Contours

The core-plus-tail model has been convolved with the statistical uncertainty from the χ^2 -minimization process to produce probability maps for each GRB localized by GBM since January 2014. Figure 3 shows an example of the maps with the contours containing the 68%, 95%, and 99.8% probability for a GRB with a fairly large statistical uncertainty. These maps and the ASCII data for the probability contours that populate them are now uploaded to the *Fermi* Science Support Center upon production of the HitL location ¹. Three GBM localization maps observed in tiling mode by iPTF resulted in afterglow detections and subsequently determined redshifts: GRB 130702A (GCN 14967), GRB 131011A (GCN 15324), and GRB 131231A (GCN 15653).

Figure 3: Probability map for the localization of GRB 080714745, with the statistical uncertainty contours (black) overlaid with the total uncertainty using the best model defined in [3]. The contours are 68%, 95%, and 99.8% confidence level regions around the χ^2 minimum from the GBM localization process.



¹http://heasarc.gsfc.nasa.gov/FTP/fermi/data/gbm/triggers/yyyy/bnyymmddfff/quicklook/glg_locplot_all_bnyymmddfff.png and [glg_loclist_all_bnyymmddfff.txt](http://heasarc.gsfc.nasa.gov/FTP/fermi/data/gbm/triggers/yyyy/bnyymmddfff/glg_loclist_all_bnyymmddfff.txt) where yyyy, mm, dd, fff are the year, month, day, and fraction of day for the GRB trigger, e.g., http://heasarc.gsfc.nasa.gov/FTP/fermi/data/gbm/triggers/2014/bn140122597/quicklook/glg_locplot_all_bn140122597.png.

References

- [1] C. A. Meegan et al., *Astrophys.J.* **702**, 791, (2009).
- [2] M. S. Briggs et al., *Astrophys.J.Supp.* **503**, 122 (1999).
- [3] V. Connaughton et al., submitted to *Astrophys.J.Supp.*